Development 133, 4151-4162 (2006) doi:10.1242/dev.02600

COUP-TFI is required for the formation of commissural projections in the forebrain by regulating axonal growth

Maria Armentano, Alessandro Filosa, Gennaro Andolfi and Michèle Studer*

The transcription factor COUP-TFI (NR2F1), an orphan member of the nuclear receptor superfamily, is an important regulator of neurogenesis, cellular differentiation and cell migration. In the forebrain, COUP-TFI controls the connectivity between thalamus and cortex and neuronal tangential migration in the basal telencephalon. Here, we show that COUP-TFI is required for proper axonal growth and guidance of all major forebrain commissures. Fibres of the corpus callosum, the hippocampal commissure and the anterior commissure project aberrantly and fail to cross the midline in *COUP-TFI* null mutants. Moreover, hippocampal neurons lacking COUP-TFI have a defect in neurite outgrowth and show an abnormal axonal morphology. To search for downstream effectors, we used microarray analysis and showed that, in the absence of COUP-TFI, expression of various cytoskeleton molecules involved in neuronal morphogenesis is affected. Diminished protein levels of the microtubule-associated protein MAP1B and increased levels of the GTP-binding protein RND2 were confirmed in the developing cortex in vivo and in primary hippocampal neurons in vitro. Therefore, based on morphological studies, gene expression profiling and primary cultured neurons, the present data uncover a previously unappreciated intrinsic role for COUP-TFI in axonal growth in vivo and supply one of the premises for COUP-TFI coordination of neuronal morphogenesis in the developing forebrain.

KEY WORDS: COUP-TFI (NR2F1), Corpus callosum, Hippocampal commissure, Anterior commissure, Axonal growth, Primary neuron culture, Gene profiling, Cytoskeleton, Knockout mice

INTRODUCTION

Within the forebrain, the major axon tracts establish stereotypical long-distance connections between different regions of the nervous system. While thalamocortical projections relay sensory information into the appropriate processing centres in the cortex, corticocortical projections allow communication between distant points of the same or contralateral hemisphere. As these pathways are essential to higher level information processing in the brain, several studies have examined the early development of these projections and have identified pioneering axonal populations, potential intermediate targets and guidance decision points for these axons (reviewed by Garel and Rubenstein, 2004; Koester and O'Leary, 1994; Rash and Richards, 2001). Due to the requirement of the major forebrain tracts to cross the midline, much attention has been focused on guidance molecules and their respective receptors, which are expressed in midline cells and in commissural tracts that have to cross the midline (reviewed by Dickson, 2002). Moreover, several transcription factors have also been shown to control the expression of membrane-bound and soluble guidance molecules involved in forebrain axon guidance, and in particular in the pathfinding of thalamocortical axons (reviewed by Lopez-Bendito and Molnar, 2003). However, how these transcriptional regulators control axonal growth and pathfinding is poorly understood.

The transcription factor COUP-TFI (chicken ovalbumin upstream promoter-transcription factor I; Nr2f1 – Mouse Genome Informatics), an orphan member of the steroid/thyroid hormone superfamily of nuclear receptors (Park et al., 2003), is involved in many processes during neuronal differentiation. The knockout mouse for *COUP-TFI* has substantially reduced thalamocortical axons projecting into the cortex (Zhou et al., 1999). It has been suggested that the abnormal thalamocortical behaviour is mainly due to intrinsic defects in the putative guidance functions of subplate neurons, their first target cells, and not to an intrinsic defect of the thalamic neurons. However, *COUP-TFI* is highly expressed in the dorsal thalamus when neurons differentiate and axons extend from the dorsal thalamus to the neocortex (Liu et al., 2000), suggesting that abnormal thalamocortical projections might derive from multiple causes. Furthermore, in view of the role of COUP-TFI in axonal projections and terminal arborization also in regions other than the forebrain (Qiu et al., 1997), COUP-TFI might be generally involved in neurite outgrowth and/or axon formation. These aspects have not yet been investigated in vivo, and nothing is known about the molecular targets of COUP-TFI that are involved in neuronal differentiation.

Here, we show that the forebrain axon guidance defects in embryos deficient for *COUP-TFI* (*COUP-TFI*^{null}) are more extensive than previously reported, and we illustrate novel aspects of COUP-TFI in the establishment of long forebrain tracts. In search of downstream targets of COUP-TFI, we have used microarray analysis and show diminished expression of *MAP1B* and, to a lesser extent, *MAP2*, two microtubule-associated proteins that regulate microtubule dynamics (Dehmelt and Halpain, 2004). Furthermore, we found that *Rnd2* (also known as *RhoN* or *Rho7*), a member of the Rho family of GTPases (Nishi et al., 1999) is highly upregulated, and that the cyclase-associated protein *CAP1*, known to regulate actin dynamics (Bertling et al., 2004) is slightly downregulated in *COUP-TFI*^{null} embryos. To assess whether abnormal expression of these factors could affect neuritogeneis and/or axogenesis in *COUP-TFI*^{null} neurons, we cultured hippocampal neurons from *COUP-TFI* mutants and revealed strong defects in neurite outgrowth and in axon morphology. *COUP-TFI*^{null} neurons become polarized but their axons tend to curl on themselves and display a high number of ectopic extensions. Altogether, these data provide strong evidence that COUP-TFI is intrinsically required for proper axonal outgrowth in the developing forebrain.

TIGEM (Telethon Institute of Genetics and Medicine), Developmental Disorders Program, Via P. Castellino 111, 80131 Napoli, Italy.

*Author for correspondence (e-mail: studer@tigem.it)

Accepted 30 August 2006

MATERIALS AND METHODS

Gene targeting and mice

We generated the *COUP-TFI*^{null} mouse line by using the Cre-lox technology. The gene targeting vector was constructed by introducing two lox sites flanking the third exon and the polyadenylation (polyA) site of the *COUP-TFI* gene, and a third lox site downstream of the selectable neomycin (neo) resistance gene. This vector contained 4.0 kb of 5′ and 1.4 kb of 3′ homologous genomic sequences, and a DTA cassette for negative selection (kind gift of P. Soriano). The targeting vector was electroporated into TBV2 embryonic stem (ES) cells according to standard protocols. We obtained 27 positive clones in which the three flox sites were correctly inserted (*COUP-TFI*^{floxneo}). Homologous recombination events were identified by Southern blot. Genomic DNA was digested with *Eco*RI and the *Xba*I-*Eco*RI fragment outside the homology arms was used as a 3′ probe (see also Fig. 1K). Another digestion with *Bam*HI and a 5′ probe within the second exon was used to confirm the right recombination event (data not shown). To obtain a null allele, two independent *COUP-TFI*^{floxneo} positive clones were electroporated with a plasmid coding for *Cre-recombinase*. Clones, in which the third exon, including the polyA, and the neo gene were excised, were screened by Southern blot and identified as *COUP-TFI*^{null} clones (see Fig. 1L). These clones were subsequently injected into C57BL/6J blastocysts and the resulting chimeras were then mated to C57BL/6J females to obtain germline transmission. *COUP-TFI*^{null} embryos were generated by crossing heterozygous animals and genotyping was performed by PCR using the following primers: forward #1 (5′-CTGCTGTAGGAATCCTGTCTC-3′), reverse #2 (5′-AATCCTCCTCGGTGAGAGTGG-3′) and reverse #3 (5′-ACATACACAGCCTGGCCTTGC-3′). For the staging of embryos, midday of the day of the vaginal plug was considered as embryonic day 0.5 (E0.5). All experiments were conducted in accordance with guidelines of the Institutional Animal Care and Use Committee, Cardarelli Hospital, Naples, Italy.

Immunohistochemistry and antibodies

The brains were sectioned and treated for immunostaining according to previously described procedures (Tripodi et al., 2004). The following antibodies were used: rabbit α-COUP-TFI (1:500); rabbit α-L1 (1:2000; kind gift of F. Rathjen); mouse α-reelin (clone G10, 1:500; kind gift of A. Goffinet); rabbit α-calbindin D-28k (clone CB38 SWANT, Bellinzona, Switzerland, 1:2500); rabbit α-calretinin (SWANT, Bellinzona, Switzerland, 1:3000), rabbit α-total MAP1B (1:100; kind gift of F. Probst), goat α-RND2/RHO7 (C-19; Santa-Cruz Biotechnology, USA, 1:100) and mouse α-TAU1 (1:500; Chemicon International). Free-floating 50 μm-thick slices from E18.5 wild-type and null brains were postfixed with 4% paraformaldehyde (PFA) for 10 minutes and treated for 20 minutes with 0.5% H_2O_2 in 96% ethanol to quench endogenous peroxidase activity. They were then preincubated in 5% goat serum, 1% BSA, 0.3% Triton X100. The sections were incubated in primary antibody (L1, 1:5000 and Calbindin, 1:5000) for 48 hours at 4°C, for 2 hours in biotinylated anti-rabbit antibody (1:200; Vector), and then processed by the ABC histochemical method (Vector). Peroxidase was visualized histochemically with diaminobenzidine (DAB). Processed sections were mounted on slides with 85% glycerol and photographed with a digital AxioCam (Zeiss).

Axonal tracing

After overnight fixation in 4% PFA, single crystals of the fluorescent carbocyanide dye DiI (1,1′-dioctadecyl 3,3,3′,3′-tetramethylindocarbocyanine perchlorate; Molecular Probes) or DiA (4-[4-(dihexadecylamino)styryl]*N*-methyl-pyridinium iodide; Molecular Probes) were placed in single or multiple locations: at E18.5 in the cortex just lateral to the midline from rostral to caudal to label callosal axons; in the CA3 hippocampal region to label the hippocampal-septal and hippocampal commissural axons; and into the anterior branch of the anterior commissure (AC). After at least 4 weeks in the dark at room temperature to allow DiI and DiA diffusion, the brains were embedded in 5% low melting agarose and cut into 100 μm-thick coronal sections on a vibratome. The sections were mounted with Vectashield with DAPI (Vector), and digital images were taken using an AxioCam (Zeiss) camera on a fluorescent microscope; they were then transferred to Photoshop (Adobe) for processing.

Microarray analysis

Brains composed of telencephalon and thalamus from 20 E14.5 embryos were dissected in cold PBS. Each brain was transferred immediately to 0.5 ml Trizol, homogenized and stored at –20°C. After genotyping, the RNA fractions were pooled into three independent replicas of wild-type and mutant brains including embryos from several litters. Matched sets of 10 μg total RNA were used for cDNA synthesis. Labelled target synthesis and hybridization to Affymetrix MOE430A 2.0. probe arrays was performed according to the protocols used at the Microarray Resource of the Boston University School of Medicine (Boston, USA) (http://gg.bu.edu/microarray/), which comply with the guidelines established by the Microarray Gene Expression Data (MGED) Society. Expression profiles were extracted using Affymetrix software (MAS 4.0, Affymetrix) to generate spreadsheets and pairwise comparisons. Each of the genes on the array was analysed for evidence of differential expression using the CyberT statistical method (Baldi and Long, 2001), which is a Bayesian extension of the traditional *t*-test. This method is well suited when there are a small number of samples and a large number of genes to test. Statistically significant differences between the three replicates in gene expression profiling was sorted by false discovery rate (FDR) using the Benjamini-Hochberg procedure (Benjamini and Hochberg, 1995).

Real-time PCR analysis

The same RNA used for the microarray analysis was reverse transcribed using the Superscript (Invitrogen) enzyme and primed with random hexamers. Real-time PCR was carried out with the GeneAmp 7000 Sequence Detection System (Applied Biosystem), with all experiments carried out in triplicate and repeated at least three times. The PCR reaction was performed using cDNA, 12.5 μl SYBR Green Master Mix (Applied Biosystem) and 400 nmol/l primer. Water was added to make a total reaction volume of 25 μl. The PCR conditions for all the genes were as follows: preheating, 50°C for 2 minutes and 95°C for 10 minutes; cycling, 40 cycles of 95°C for 15 seconds and 60°C for 1 minute. The quantification results were expressed in terms of the cycle threshold (Ct). The means of the Ct values were calculated from each triplicate. All the assays were normalized to *GAPDH*. Differences between the mean Ct values of the tested genes and those of the reference genes were calculated as $\Delta Ct_{gene}=Ct_{gene}-Ct_{reference}$ and represented as $2^{-\Delta Ct}$ values. The relative fold changes in expression levels were determined as $2^{-\Delta\Delta Ct}$. The following primer sequences were used: MAP1B (forward, 5′-CAGTCTGGCTCTTTCTCCTTCC-3′; reverse, 5′-TGTCAAGGTTGGAGTTCTTCCA-3′); MAP2 (forward, 5′-AACATCAAATACCAGCCTAAGG-3′; reverse, 5′-TGGCCTGTGACGGATGTTCT-3′); CAP1 (forward-5′-GGCTTACATCTACAAGTGTGTC-3′; reverse, 5′-TGCCCACCACGTCATCAAACAC-3′); RND2 (forward, 5′-CTCGATCCTTATGCATCTCGC-3′; reverse, 5′-ATAGGCAGCTACGTCGTACTG-3′); GAPDH (forward, 5′-GTATGACTCCACTCACGGCAAA-3′; reverse, 5′-TTCCCATTCTCGGCCTTG-3′).

Protein extracts and western blot

Brains of E14.5 and 18.5 mutant mice and control litter mates were dissected out and homogenized in 125 mmol/l Tris, pH 6.8, 2% SDS, 1 mmol/l PMSF, followed by boiling to lower the viscosity. After centrifugation, the supernatants were analysed by western blot. Protein samples were resuspended in SDS sample buffer (20 mmol/l Tris-HCl, pH 6.8, 2% SDS, 5% β-mercaptoethanol, 2.5% glycerol and 2.5% bromophenol blue) and subjected to standard SDS-PAGE electrophoresis followed by transfer to a polyvinylidene difluoride membrane (PVDF, Amersham). All labelling was visualized with Super Signal West Pico Chemiluminescent Substrate (PIERCE, Perbio) except for RND2 immunoblotting, which was detected according to the standard procedures suggested in the Vectastain ABC kit (Vector Laboratories). The following antibodies were used in the TTBS blocking solution (1× TBS, 0.1% Tween) with 5% skimmed milk: total MAP1B rabbit polyclonal (1:600; kind gift of F. Propst); SMI31 mouse monoclonal (1:1000; Sternberger Monoclonals); MAP1B clone 125 mouse monoclonal (1:150; kind gift of J. Avila); GSK3β mouse monoclonal (1:1000; kind gift of J. Avila and E. Soriano); P-Tyr-GSK3β mouse monoclonal (1:1000; kind gift of J. Avila and E. Soriano); P-Ser-GSK3β mouse monoclonal (1:1000; kind gift of J. Avila and E. Soriano); CDK5

mouse monoclonal (1:1000; kind gift of J. Avila); MAP2 clone HM-2 mouse monoclonal (1:500; SIGMA); RND2/RHO7 goat polyclonal (C19; 1:100; Santa Cruz Biotechnology); CAP1 guinea pig polyclonal (1:1500; kind gift of P. Lappalainen); TAU1 mouse monoclonal (1:2000; Chemicon International); NFM145 rabbit polyclonal (1:1000; Chemicon International). PVDF membranes were incubated with the above-listed primary antibodies in blocking solution at 4°C overnight. The secondary peroxidase-labelled antibodies (Amersham Biosciences) were used at a concentration of 1:3000 in TTBS, 5% skimmed milk. All of the western blot data represent a minimum of three separate experiments.

Primary cultures

For the preparation of primary hippocampal cultures, E18.5 embryos were removed aseptically from pregnant mice and placed in individual sterile petri dishes. The tails from individual embryos were kept for genotyping. Dissociated cultures of hippocampal pyramidal cells were then prepared as previously described (Banker and Cowan, 1977). Briefly, the hippocampal tissue was isolated and digested with 2.5% trypsin for 10 minutes at 37°C, followed by trituration with pipettes in the plating medium (Neurobasal medium including 10% horse serum, 0.1 mmol penicillin/streptomycin, glutamine 2 mmol, pyruvate 1 mmol, GIBCO). Dissociated neurons were plated onto permanox chamber slide coated with poly-D-lysine at a density of 50,000-70,000 cells/mm^2. After culturing for 6 hours, media were changed into neuronal culture medium (Neurobasal medium supplemented with 2% B27 and 1% N2, GIBCO). Standard immunofluorescence procedures were used to process the neuronal cultures at 12, 24 and 48 hours after plating (Gonzalez-Billault et al., 2002). We used a monoclonal antibody against tyrosinated α-tubulin (1:1100, clone TUB-1A2, mouse IgG, Sigma), and rhodamine-phalloidin (Molecular Probes) was included with the secondary antibody to visualize F-actin. Total MAP1B rabbit polyclonal (1:600), TAU1 mouse monoclonal (1:300) and the RND2/RHO7 goat polyclonal (1:100) antibodies were used in neuronal cultures at 24 and 48 hours after plating. Cells undergoing apoptotic cell death were detected by TUNEL analysis using the Apop-Tag Kit (Chemicon) according to the supplier's instructions.

Morphological quantification, cell counting and statistical analysis

The relative size of the cingulate cortex and the thickness of the AC were quantified using Image J software. In the primary culture experiments, the fluorescence cells were acquired with a light-sensitive charge-coupled device (CCD) digital camera DFC350 FX (Leica, Germany). For fluorescence quantification, a FW4000 Imaging software system (Leica, Germany) was used on acquired cells. To quantify fluorescence intensity, neurons were double stained with MAP1B and TAU. TAU was used as an internal control because protein levels were not altered. In each independent experiment, 15-20 neurons were selected, and measurements were performed within the soma and neurites using a standardized area. The total fluorescence intensity expressed in pixels/area was measured and the background measurement was then subtracted. The final result was displayed as average fluorescence intensity per area unit. All the data were analysed and graphs were constructed using Microsoft Excel software. All error bars represent the standard error of the mean (s.e.m.). Statistical significance was determined using two-tailed Student's *t*-tests. $*P<0.05$, $**P<0.01$.

RESULTS

COUP-TFI is localized in regions associated with the major forebrain neuronal tracts

We have previously shown that at E13.5, COUP-TFI is uniformly present across the whole pallium (Tripodi et al., 2004). At E15.5, COUP-TFI expression was maintained throughout the radial extent of the cortex, with the highest expression in the subplate and cortical plate, from which the main corticofugal neurons differentiate, but also in the ventricular and subventricular zones (Fig. 1B-D). In rostro-medial sections, COUP-TFI expression showed a clear pallial/subpallial boundary, along which the ventral pallium radial migratory stream (Medina et al., 2004) of positive cells forms a curved band (Fig. 1B). COUP-TFI was also detected in the region of the internal capsule through which thalamocortical axons pass before projecting into the cortex (Fig. 1C,D). In the future cingulate cortex, COUP-TFI was localized in sparse cells in the cortical plate, close to the marginal zone (Fig. 1E). Double-immunofluorescence with Reelin, a marker of the marginal zone, showed that COUP-TFI-positive cells were Reelin-negative (Fig. 1F), and thus positioned in deeper cell layers that were reminiscent of the position of callosal pioneer neurons (Koester and O'Leary, 1994; Rash and Richards, 2001). Moreover, COUP-TFI was localized in the anterior olfactory nucleus (Fig. 1A), which together with the piriform cortex represents the main population of neurons that will form the anterior limb of the AC (Jouandet and Hartenstein, 1983). Interestingly, COUP-TFI was also located in the nucleus of the lateral olfactory tract (data not shown) and various pallial subnuclei of the claustroamygdaloid complex (Fig. 1C,D), from which the posterior limb component of the AC originates.

At caudal levels expression of COUP-TFI was high in the primordia of the hippocampus and dorsal thalamus at a stage when neurons start to differentiate. Expression of COUP-TFI in the diencephalon was observed at E13.5 in all thalamic progenitors (Fig. 1G). At E15.5 COUP-TFI was maintained in the whole dorsal thalamus at high levels (Fig. 1H) and at E18.5 when individual thalamic nuclei are better defined, COUP-TFI was expressed mainly in the lateral geniculate and ventroposterior nuclei (Fig. 1I,J and data not shown). Furthermore, at E18.5, when the various layers of the hippocampus can be better identified, strong staining of COUP-TFI was observed in the hippocampal plate, in the subplate and in the intermediate zone (Fig. 1I). Sparse COUP-TFI-positive cells were also seen in the inner marginal zone, a layer rich in GABAergic interneurons.

Taken together, these data show that in the developing forebrain, COUP-TFI is located in regions from which the major forebrain neuronal tracts originate.

Targeting of the *COUP-TFI* locus

As shown above, COUP-TFI is highly and dynamically expressed in many regions of the forebrain from which neurons depart and arrive; however, axonal pathfinding defects in the forebrain have been described only for thalamocortical axons in *COUP-TFI* null mice (Zhou et al., 1999). It is therefore not clear whether COUP-TFI plays a unique role in the guidance of thalamocortical afferent neurons and brain regionalization (Zhou et al., 2001), or alternatively whether it is more generally involved in axogenesis. To challenge this question, we used a strategy of gene targeting through homologous recombination in ES cells that allowed us to obtain at the same time *COUP-TFI* floxed (*COUP-TFI*^{flox}) and *COUP-TFI* knockout (*COUP-TFI*^{null}) mice (Fig. 1K and data not shown). In this paper, we will only report the generation and phenotypic analysis of the *COUP-TFI*^{null} mice. Data obtained from the *COUP-TFI*^{flox} mated with tissue-specific Cre-recombinase mice will be presented in another report (M.A. and M.S., in preparation).

To target the *COUP-TFI* gene, two lox sites were inserted upstream and downstream of the third exon and part of the 3′ untranslated region including the polyA sites, while a third lox site was inserted downstream of the selectable marker *neomycin* (*neo*) gene, resulting in the *COUP-TFI*^{floxneo} allele (Fig. 1K and Materials and methods). In the presence of the *Cre-recombinase* in ES cells, the two external lox sites recombined, resulting in the excision of the third exon and the polyA sites, as demonstrated by Southern blot and PCR using specific primers for either the *COUP-TFI* wild-type or the *COUP-TFI*^{null} alleles (Fig. 1L,M). Complete lack of COUP-TFI protein was obtained in homozygous *COUP-TFI*^{null} animals, as

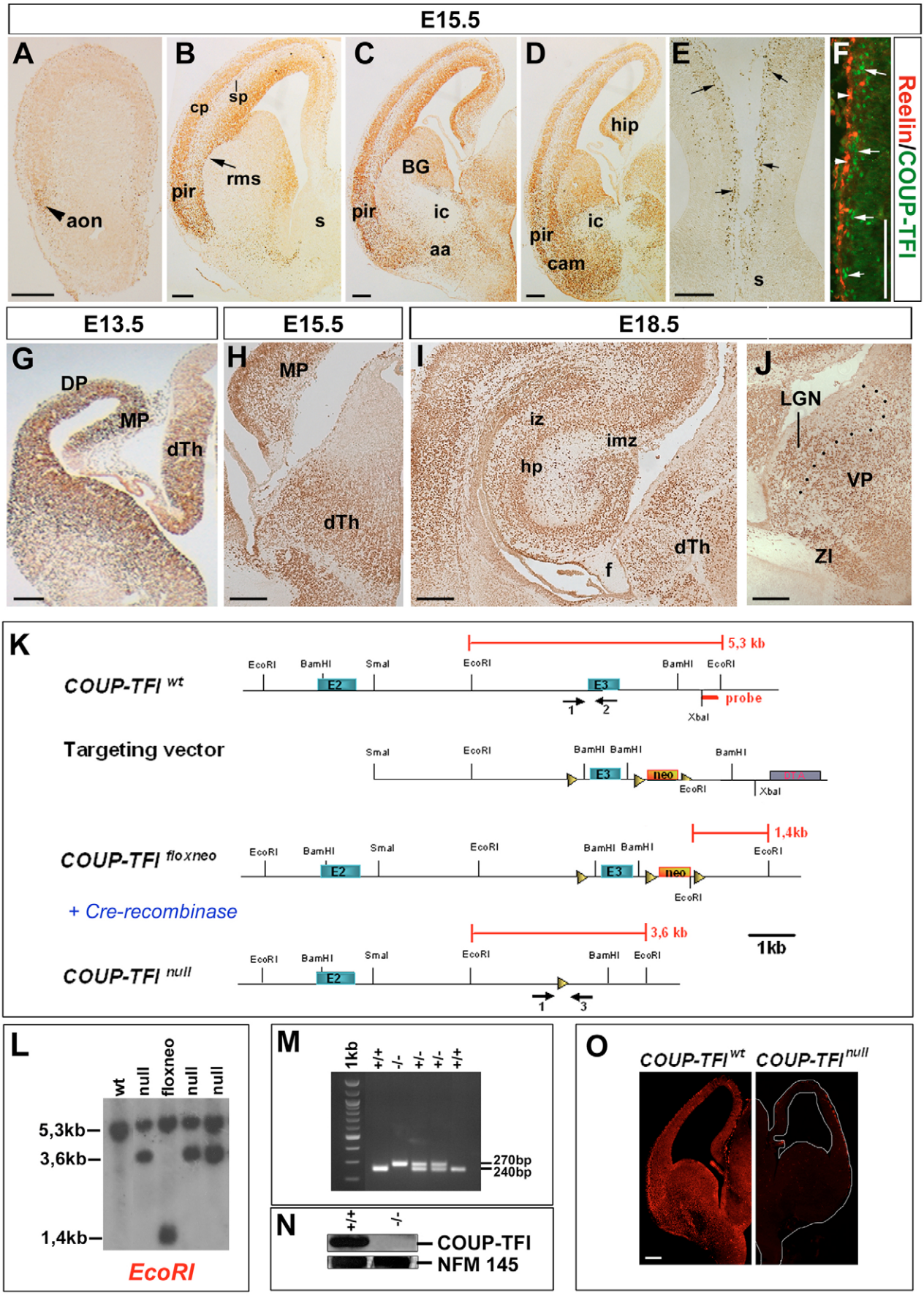

Fig. 1. See next page for legend.

Fig. 1. Expression and inactivation of COUP-TFI in the developing forebrain. (**A-J**) Coronal sections immunostained for COUP-TFI at the ages indicated above. A to D are consecutive rostral to caudal sections. (E) Enlargement of the presumptive cingulate cortex in which COUP-TFI is present in scattered cells (arrows). (F) Detail of one half of the cingulate cortex, double immunolabelled for COUP-TFI (green) and Reelin (red), shows that COUP-TFI-positive cells do not co-localize with the marginal zone marker Reelin. (G-J) Note how COUP-TFI starts to be expressed in the dorsal thalamus (dTh) from the onset of thalamic differentiation and is maintained at later stages in distinct nuclei. (I) In the hippocampus high levels of COUP-TFI are present in the hippocampal plate and in the intermediate zone. Scattered cells are also detected in the inner marginal zone. (J) Detail of the dorsal thalamic region in a section posterior to (I) shows high expression of COUP-TFI in the lateral geniculate and ventroposterior nuclei. Dashed lines demarcate the LGN and VP thalamic nuclei. The zona incerta is also positive for COUP-TFI. (**K**) Diagram showing the gene targeting strategy used to obtain the *COUP-TFI*^{null} allele after Cre-recombination in embryonal stem cells. The lox P sites are depicted as triangles. Blue boxes represent exons. Appropriate restriction enzyme sites are indicated. Red lines indicate the expected fragment size after *Eco*RI digestion of *COUP-TFI*^{wt}, *COUP-TFI*^{floxneo} and *COUP-TFI*^{null} genomic DNA, as shown in a Southern blot (**L**). (**M**) PCR genotyping on wild-type (+/+), heterozygous (+/–) and homozygous (–/–) mice using the primers indicated in K as black arrows. (**N**) Western blot shows total absence of COUP-TFI protein in homozygous mutant animals. (**O**) Coronal sections of wild-type and homozygous E15.5 embryos confirm complete absence of COUP-TFI protein in homozygous brains. Scale bars: 200 μm. aa, anterior amydgaloid area; aon, anterior olfactory nucleus; BG, basal ganglia; cam, claustro-amygdaloid complex; cp, cortical plate; hip, hippocampus; hp, hippocampal plate; ic, internal capsule; imz, inner marginal zone; iz, intermediate zone; LGN, lateral geniculate nuclei; pir, piriform cortex; rms, radial migratory stream; s, septum; sp, subplate; VP, ventroposterior nuclei; ZI, zona incerta.

shown by western blot and E15.5 telencephalic sections (Fig. 1N,O), and thus these animals could be considered complete null mutants. In this line, maintained mainly on a C57Bl/6 background, all homozygous pups for the *COUP-TFI*^{null} mutations died at perinatal stages and no animals were obtained after weaning.

Abnormal development of midline commissural projections in *COUP-TFI*^{null} brains: the corpus callosum and the hippocampal commissure

In view of the expression of COUP-TFI in the major developing commissural neurons, we examined the morphology of these projections in our *COUP-TFI*^{null} mouse line. At E18.5, when a significant number of axons have normally crossed the midline (Fig. 2A,B), the callosal projections failed to show decussation in the majority of *COUP-TFI*^{null} fetuses (n=12/19), and stopped abruptly at the midline (Fig. 2A′,B′). Furthermore, the mutant embryos presented a ventrally extended cingulate cortex, as confirmed by the ventrally extended localization of calretinin in the cingulum bundle (Fig. 2A′), and a significantly extended length of the medial cortex (Lc), compared with the total dorsoventral (DV) length of the telencephalon (Lt in Fig. 2F: 36.3±1.3% in wild type, 47.2±3.2% in null embryos; P=0.04). In three out of 19 cases, there was a partial cross, and the non-crossing commissural fibres had an abnormal defasciculated aspect (Fig. 2C′,D′ and insets). To understand whether there was a difference in the anteroposterior (AP) distribution of callosal projections, DiA was injected into the anteromedial and DiI into the posteromedial neocortex (Fig. 3A,B and inset); at all levels callosal projections formed aberrantly oriented fibres, known as Probst bundles in *COUP-TFI*^{null} brains (Fig. 3A′,B′; n=6). Furthermore, null brains failed to show a segregation of anterior (DiA; green) versus posterior (DiI; red) projections as observed in wild-type embryos (Fig. 3A,B; n=6), such that green fibres were found posteriorly, and red fibres were identified anteriorly (Fig. 3A′,B′), suggesting that callosal bundles projected abnormally along the AP axis.

Finally, in the region of the splenium L1 labelled three distinct projections in wild-type embryos, with the callosal axons crossing dorsal to, and the fornix ventral to, the hippocampal commissure (Fig. 2E). In the absence of COUP-TFI, the axonal tracts stopped at the level of the midline (Fig. 2E′ and inset). DiI labelling from the hippocampus confirmed the failure of the hippocampal commissure to cross the midline in *COUP-TFI*^{null} brains and showed the presence of ventrally oriented thick ectopic bundles (Fig. 3D′,E′).

In summary, our data suggest a role for COUP-TFI in the formation of the midline commissural projections at both AP and DV levels. In the absence of *COUP-TFI*, the corpus callosum and the hippocampal commissures were stunted at the midline, and all hippocampal fibres formed a thick bundle together with the fornix, which showed aberrant growth into the septal region.

Abnormal branching and fasciculation of the AC in *COUP-TFI*^{null} mice

The AC is a prominent commissure in the brain and it interconnects the basal telencephalon and olfactory pallial structures of the two hemispheres. It is comprised of an anterior limb, a horseshoe-shaped tract connecting the two olfactory bulbs, a posterior limb that forms a laterally directed tract entering into the external capsule and carrying projections between the two temporal lobes, and the commissural component of the stria terminalis (Jouandet and Hartenstein, 1983). In view of the expression of COUP-TFI in most of the neurons giving rise to the various components of the AC (Fig. 1), we produced a series of coronal and horizontal sections immunostained with anti-L1 in E18.5 wild-type and *COUP-TFI*^{null} embryos (Fig. 4). Coronal sections at rostral levels indicated the presence of the anterior limb branches in the olfactory cortex (Fig. 4A,B) in wild-type and null fetuses. However, the number of these branches was increased in the *COUP-TFI*^{null} embryos (Fig. 4A′,B′). Horizontal sections showed that both anterior and posterior branching were abnormally positioned dorsoventrally in the mutant embryos and innervated the anteromedial cortex through numerous tracts (Fig. 4H′,I′). This dorsoventral shift of the two different branches resulted in a thicker commissural tract, as confirmed by direct measurements of the AC tract in coronal and horizontal sections of wild-type and null embryos (Fig. 4J; coronals: 147±12 μm in wild type, versus 195±5 μm in null embryos; P=0.044; horizontals: 146±6 μm in wild type versus 237±12 μm in null embryos; P=0.004).

In 12 of the13 null embryos examined, some AC fascicles also showed aberrant connections with the hippocampal commissure. To better understand this defect, we traced the hippocampal projections and the AC with different colours (Fig. 4E,F). The origin of the misrouted projections derived from both commissures, although they followed distinct paths (Fig. 4E′,F′). Therefore, our results show that COUP-TFI is involved in the development of the AC through the correct positioning and guiding of its anterior and posterior branches, and its midline decussation. Together with the deficiencies observed in the corpus callosum and the hippocampal commissure, our data show that all of the major forebrain commissures have guidance abnormalities along the AP and DV axes of *COUP-TFI*^{null} mutants.

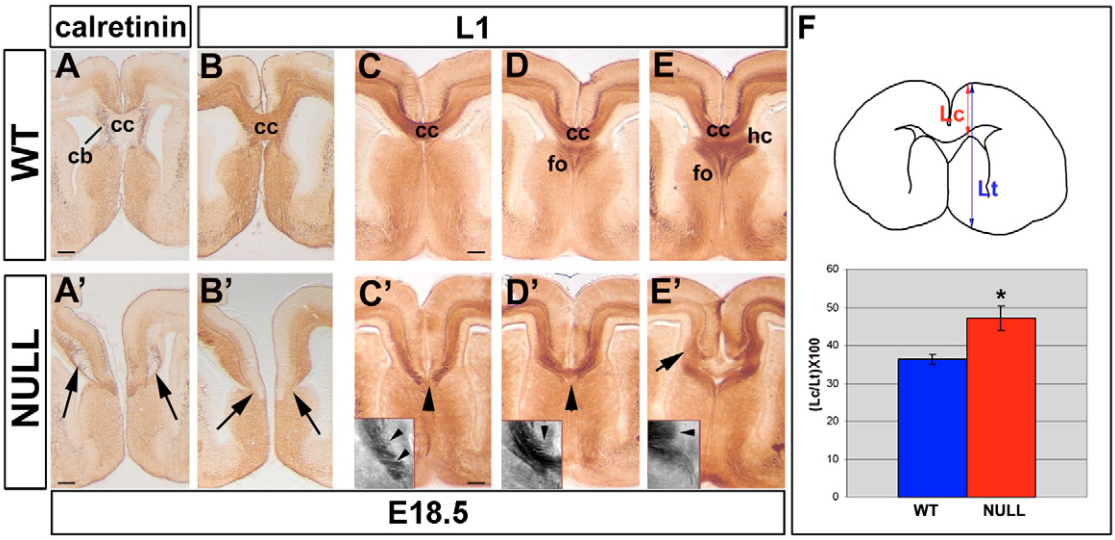

Fig. 2. Abnormal development of the corpus callosum and hippocampal commissure in *COUP-TFI*^{null} brains. Coronal sections through the telencephalon of wild-type and *COUP-TFI*^{null} embryos at the stages indicated and immunostained for calretinin (**A**,**A′**) and L1 (**B-E′**). (A-B′) At E18.5 corpus callosum fibres cross the midline in wild-type embryos (A,B), but remain ipsilateral in null mutants (A′,B′). Note how the cingulate cortex and the cingulum bundle are ventrally extended in the null mutants (arrows in A′,B′). This phenomenon is quantified in **F**, where the length of the cingulate cortex is compared to the total DV length of the forebrain. (C′-E′) Serial rostrocaudal sections of E18.5 embryos indicate a milder phenotype in 3/19 null mutants. Arrowheads in C′,D′ point to partial crossing. (E′) In more caudal sections the mutants lack a morphologically distinct corpus callosum and hippocampal commissure (arrow). The arrowheads in the insets C′-E′ indicate defasciculated fibres stopping abruptly at the midline. Scale bars: 200 μm. cb, cingulum bundle; cc, corpus callosum; fo, fornix; hc, hippocampal commissure; Lc, length of the cingulate cortex; Lt, total DV length of the forebrain; NULL, *COUP-TFI*^{null} embryos; WT, wild-type embryos.

Identification of microtubule- and actin-regulating factors as COUP-TFI downstream effectors

To determine the potential downstream targets of COUP-TFI that would explain the basis of these axon guidance defects, we performed a microarray analysis using the Affymetrix mouse genomic array (MOE 430 2.0 A). As target RNA, we used the dissected telencephali and thalami of E14.5 wild-type and null embryos. The choice of E14.5 was based on the knowledge that at this stage, most of the forebrain projections begin to be established and the molecules involved in axon pathfinding are highly expressed. As expected, the gene that had the highest fold change (318) and was the first most differentially expressed gene between the wild-type and the null brains was *COUP-TFI* itself. Interesting candidates that had a highly significant *P*-value were the microtubule-associated protein *MAP1B* (Kutschera et al., 1998) with a 2.5-fold change ($P=4\times10^{-6}$), the small GTP-binding protein *Rnd2* (Nishi et al., 1999) with a 1.7-fold change ($P=3\times10^{-7}$), and the adenylate cyclase-associated protein *CAP1* (Bertling et al., 2004) with a 1.5-fold change ($P=5\times10^{-5}$). In addition, with a slightly lower FDR (0.155), but a highly significant *P*-value of 4×10^{-4}, there was the microtubule-associated protein *MAP2* (Kalcheva et al., 1995) (1.7-fold change). Interestingly, all of these genes are components of the cytoskeleton machinery and are highly expressed in the forebrain during neuronal morphogenesis; indeed, they have been implicated in neurite outgrowth and neurite branching.

To validate the microarray data, the $2^{-\Delta\Delta CT}$ method (Livak and Schmittgen, 2001) was used to calculate the relative changes in gene expression from real-time quantitative RT-PCR (QRT-PCR). The data shown in Fig. 5A are presented as fold changes in gene expression, which were normalized to an endogenous reference gene, relative to the wild-type brains as control, which were designated as 1.0. We confirmed that expression levels of *MAP1B* and *MAP2* decreased to 0.6±0.09 ($P=0.007$) and 0.8±0.08

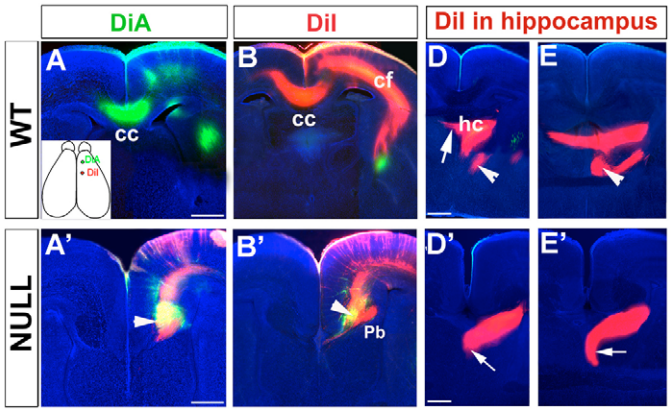

Fig. 3. Aberrant projections of the corpus callosum and hippocampal commissure in *COUP-TFI*^{null} brains. Coronal sections through the telencephalon of E18.5 wild-type and *COUP-TFI*^{null} fetuses in which DiA was implanted in the rostromedial neocortex (**A**,**A′**) and DiI in a more caudomedial position (**B**,**B′**). The inset in A indicates the positions of the dyes. Note the presence of Probst bundles (arrowheads in A′,B′) in the ipsilateral cortex. (**D-E′**) Consecutive rostrocaudal sections, in which DiI was inserted in the hippocampus, show how the hippocampal commissure fails to cross in null mutants (arrows in D′,E′). At all levels, labelled fibres do not cross the midline but turn ventrally. The white arrowheads in D and E indicate some retrogradely labelled neurons in the medial septum/diagonal band complex. Scale bars: 200 μm. NULL, *COUP-TFI*^{null} fetuses; Pb, Probst bundles; WT, wild-type fetuses.

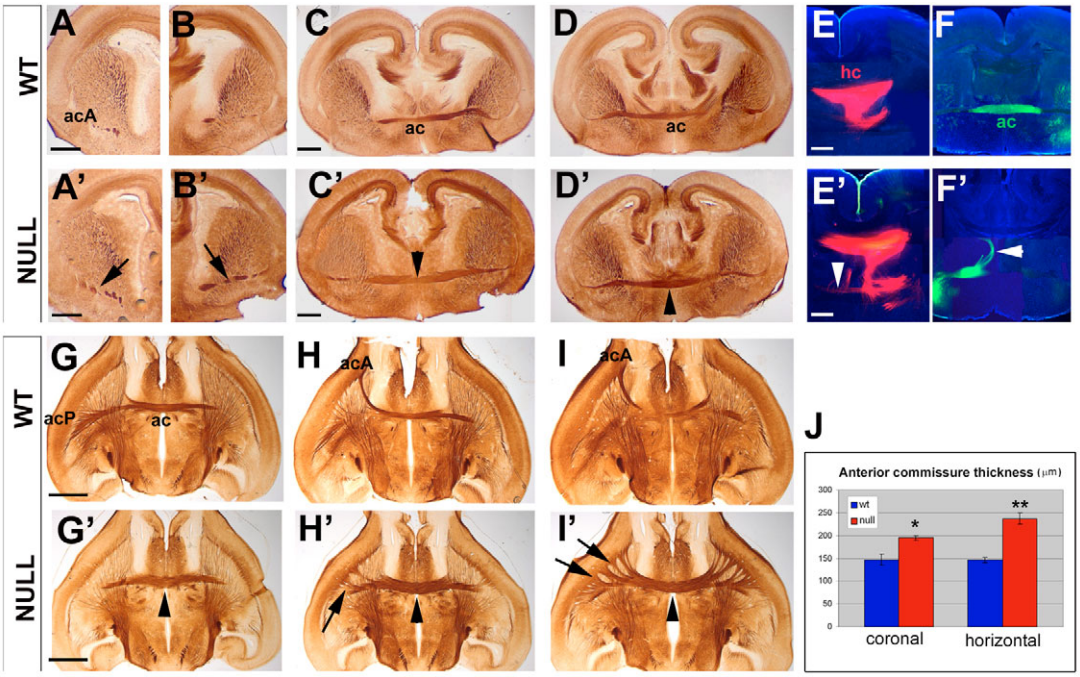

Fig. 4. Abnormal axon trajectories in the AC of *COUP-TFI*^{null} brains. Serial free-floating coronal (**A-D′**) and horizontal (**G-I′**) sections through the telencephalon of E18.5 wild-type and *COUP-TFI*^{null} fetuses immunostained for L1. In wild-type embryos, the anterior tract of the AC is visible as distinct spots in anterior coronal sections (A,B) and as a horseshoe-shaped tract in horizontal sections (H). The posterior tract is positioned more dorsally than the anterior one and forms a laterally directed tract connecting the two temporal lobes (G). The two tracts show decussation jointly at the midline (C,D,G). In the *COUP-TFI*^{null} brains, the anterior and posterior tracts form ectopic fascicles that innervate the rostromedial cortex (arrows in H′,I′). The main tract shows decussation at the midline but its overall diameter is larger (arrowheads in C′,D′,G′,H′,I′). The arrows in A′ and B′ indicate ectopic fascicles of the anterior tract in rostral sections. (**E-F′**) Double dye tracing of E18.5 brains in which a crystal of DiI was placed in the hippocampus (E,E′) and a crystal of DiA was placed in the anterior branch of the AC (F,F′). Note that in the null embryos hippocampal-septal projections enter the AC tract (arrowhead in E′) and the AC fibres project dorsally towards the hippocampal commissure (arrowhead in F′). (**J**) Quantification of the thickness of wild-type (blue) and null (red) AC measured at the midline. In the null embryos, the AC is significantly larger in both the coronal and horizontal planes. Scale bars: 200 μm. acA, anterior tract of the AC; acP, posterior tract of the AC; NULL, *COUP-TFI*^{null} fetuses; WT, wild-type fetuses.

(P=0.002), respectively, and *CAP1* mRNA decreased to 0.7±0.14 (P=0.012), while *Rnd2* mRNA levels increased to 2.1±0.2 (P=0.003).

To assess whether protein levels of target genes were affected in null embryos, we performed western blot on protein extracts from E14.5 and E18.5 wild-type and *COUP-TFI*^{null} brains (Fig. 5B and data not shown). We used an antibody that recognizes the total amount of MAP1B, independently of its phosphorylation state (Fischer and Romano-Clarke, 1990), and specific antibodies that distinguish the two types of MAP1B phosphorylation: the SMI31 monoclonal antibody for mode I (Johnstone et al., 1997), and the 125 monoclonal antibody specific to mode II (Ulloa et al., 1993). The protein levels of all MAP1B forms were reduced in the *COUP-TFI*^{null} brains (Fig. 5B); however, levels of the glycogen synthase kinase 3β (GSK3β) and cyclin-dependent kinase 5 (CDK5) kinases were not modified in the null brains, confirming that the diminished levels of MAP1B are exclusively due to decreased transcriptional regulation of *MAP1B* mRNA. By using an antibody against all the MAP2 isoforms, we detected no differences in the high molecular weight isoform MAP2a/b, and a slightly reduced level in the embryonic isoform MAP2c (Fig. 5B), consistent with the minor decrease in transcriptional regulation (Fig. 5A). A slight decrease in protein levels was also observed with the CAP1 antibody, whereas RND2 increased significantly, in accordance with the differences observed in transcript levels (Fig. 5A,B). No differences in TAU proteins were observed between wild-type and null brains, suggesting that COUP-TFI regulates the expression of only a subset of microtubule-associated proteins.

Finally, we assessed whether protein levels of MAP1B and RND2, the two factors that showed the highest difference between wild-type and mutant brains, were specifically altered in the cortical plate of E15.5 brains. On the one hand, as observed in Fig. 5C-E′, levels of MAP1B protein in the marginal and upper intermediate zones were diminished in the *COUP-TFI*^{null} brains (see asterisk and arrow in Fig. 5C and C′), while no changes were detected in the lower intermediate zone. On the other hand, protein levels of RND2 were increased in the same layers (Fig. 5D,D′) and RND2 was also expanded dorsally in the upper intermediate zone (arrow in Fig. 5D′). Distribution of the TAU protein was unchanged in the marginal and intermediate zones (Fig. 5E,E′), consistent with the data from the western blot.

In summary, our results show that at the mRNA and protein levels, expression of various cytoskeletal molecules involved in axon guidance and neuronal migration are perturbed in the absence of COUP-TFI.

Inhibition of neurite outgrowth in cultured primary neurons of *COUP-TFI*^{null} brains

Previous reports have shown that in the developing cortex MAP1B is required for proper axon growth (Gonzalez-Billault et al., 2001; Goold and Gordon-Weeks, 2001; Goold and Gordon-Weeks, 2005),

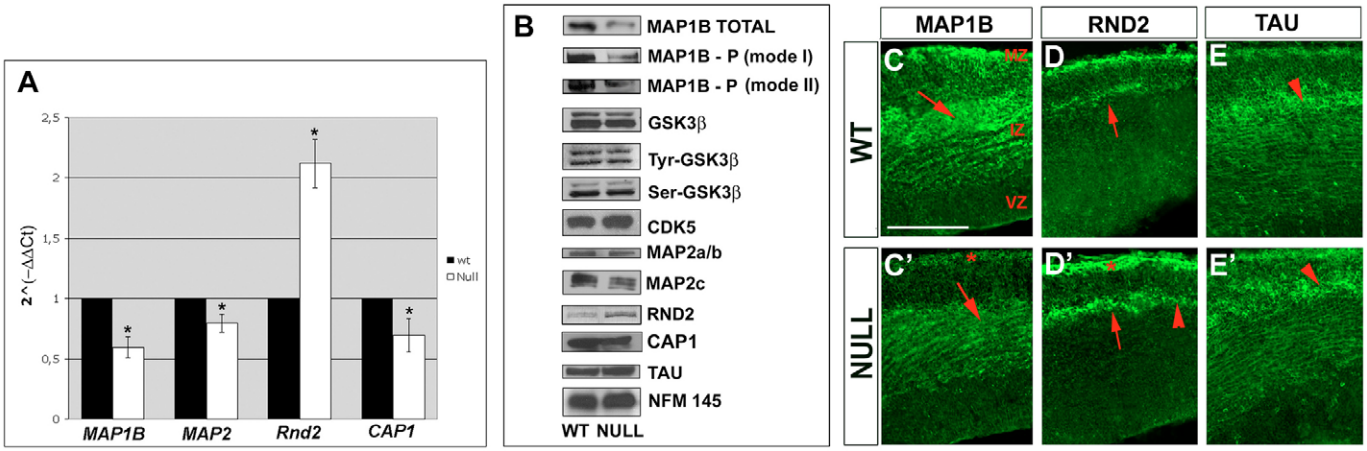

Fig. 5. Altered gene expression and protein levels of actin and microtubule cytoskeleton molecules in *COUP-TFI*^{null}. (**A**) Fold-change variations (expressed as $2^{-\Delta\Delta Ct}$ values) in *MAP1B, MAP2, Rnd2* and *CAP1* mRNA expression levels between the wild-type and *COUP-TFI*^{null} E14.5 brains after QRT-PCR. The data are normalized to levels of expression of all of the genes in wild-type embryos as 1.0. Significant differences are indicated by asterisks. (**B**) Western blots of E14.5 brain extracts from wild-type and *COUP-TFI*^{null} littermates. The blots were incubated with the antibodies listed on the right-hand side. (**C-E′**) Coronal sections of E15.5 wild-type and *COUP-TFI*^{null} dorsolateral cortices immunostained for MAP1B, RND2 and TAU antibodies. (C′,D′) The arrows indicate reduced MAP1B and increased RND2 protein levels in the upper intermediate zone, respectively. The asterisks show altered expression in the marginal zone and the arrowhead in D′ points to an expanded expression of RND2 into more dorsal regions. (E,E′) The arrowheads show no changes in expression levels of the general microtubule-associated protein TAU. Scale bar: 200 μm. IZ, intermediate zone; MZ, marginal zone; NULL, *COUP-TFI*^{null} fetuses; VZ, ventricular zone; WT, wild-type fetuses.

while RND2 is associated with the morphological changes of pyramidal neurons (Nakamura et al., 2006). To determine whether *COUP-TFI*^{null} pyramidal neurons had morphological alterations, we used the well-established system of cultured hippocampal pyramidal neurons (Bradke and Dotti, 2000; Craig and Banker, 1994). The development of primary hippocampal neurons in vitro has been classified into distinct morphological stages according to the progress of neurite outgrowth (Dotti et al., 1988). In the first 6 hours of culture, the majority of neurons remain spherical (Fig. 6A); neurites start to grow out 12 to 24 hours after plating, although they have no visible polarization and a star-like morphology (Fig. 6D). After 24 to 48 hours in culture, virtually all the neurons become polarized, displaying long, thin axons and several much shorter processes or minor neurites (Fig. 6F).

To characterize the morphology of *COUP-TFI*^{null} hippocampal neurons in culture, we used the time points described above and stained neurons for tubulin and actin. Twelve hours after plating, the majority of *COUP-TFI*-deficient neurons had either no protrusions or a slightly elongated process and showed abnormal distribution of actin around the cell body (Fig. 6B′,B″). At a time when the wild-type neurons showed a clear symmetrical distribution of neurites tipped with growth cones (Fig. 6D), the *COUP-TFI*-deficient neurons had either no processes or abnormal neurites, which tended to curl up on themselves (Fig. 6E). The percentage of neurons that presented no, or very little, outgrowth was quantified in the wild-type and null cultures (Fig. 6C). The number of abnormal neurons was significantly higher in null cultures until 48 hours after plating [12 hours, 14% ±7 in wild type (n=451) versus 68% ±11 in null (n=477), P=0.03; 24 hours, 6% ±0.6 in wild type (n=737) versus 35% ±2 in null (n=680), P=0.004; 48 hours, 2% ±0.7 in wild type (n=625) versus 23% ±1 in null (n=813), P=0.01]. After 60 hours, the number of spherical neurons was similar in both the wild-type and null cultures (1% ±0.5 in wild type (n=632) versus 3% ±0.4 in null (n=442), P=0.08), suggesting that either most of these neurons were delayed or that they died. With the help of the TUNEL assay, we could not detect any significant increase of apoptotic neurons from 12 to 60 hours in culture (data not shown), suggesting that neurite outgrowth might have been delayed in *COUP-TFI*-deficient neurons. However, axon morphology was strongly affected, and neurons displayed numerous short filopodial extensions and growth-cone-like structures around the cell body and neurites (Fig. 6G-G″). Moreover, the axons rolled up in an abnormal fashion and tubulin-positive structures accumulated abnormally around the cell body (Fig. 6G-G″). Nevertheless, *COUP-TFI*-deficient neurons showed no statistical difference in neurite length from the wild-type neurons after 72 hours in culture (data not shown).

In summary, our data demonstrate that the hippocampal neurons from *COUP-TFI*^{null} brains have a selective and significant delay in neurite outgrowth and abnormal axonal morphology.

MAP1B levels are decreased and RND2 is ectopically expressed in COUP-TFI-deficient neurons

To better understand whether the axonal defects described above were correlated with an abnormal distribution of MAP1B and RND2 proteins in cultured neurons, we stained primary hippocampal neurons for both proteins 24 and 48 hours after plating (Fig. 7). As previously described (Boyne et al., 1995), total MAP1B is normally distributed uniformly in the cell body and in the developing neurites, similarly to TAU (Fig. 7A-A″). In *COUP-TFI*^{null} neurons, MAP1B levels were downregulated mainly in the growing axons, although a slight reduction was also observed in the soma, whereas levels of TAU were not altered (Fig. 7B-B″,C). The fluorescence intensity of MAP1B and TAU, expressed in pixels/area, was independently quantified in the soma and in the axons of wild-type and null neurons (Fig. 7C). A significant decrease in MAP1B protein levels, particularly in the growing axons, was confirmed at the statistic level (TAU in soma, 174.7±3.6 in wild type versus 171.2±0.7 in null, P=0.44; TAU in axon, 162.6±2.1 in wild type versus 165.1±2.5 in null, *P=0.45*; MAP1B in soma, 175.8±4.0 in wild type versus

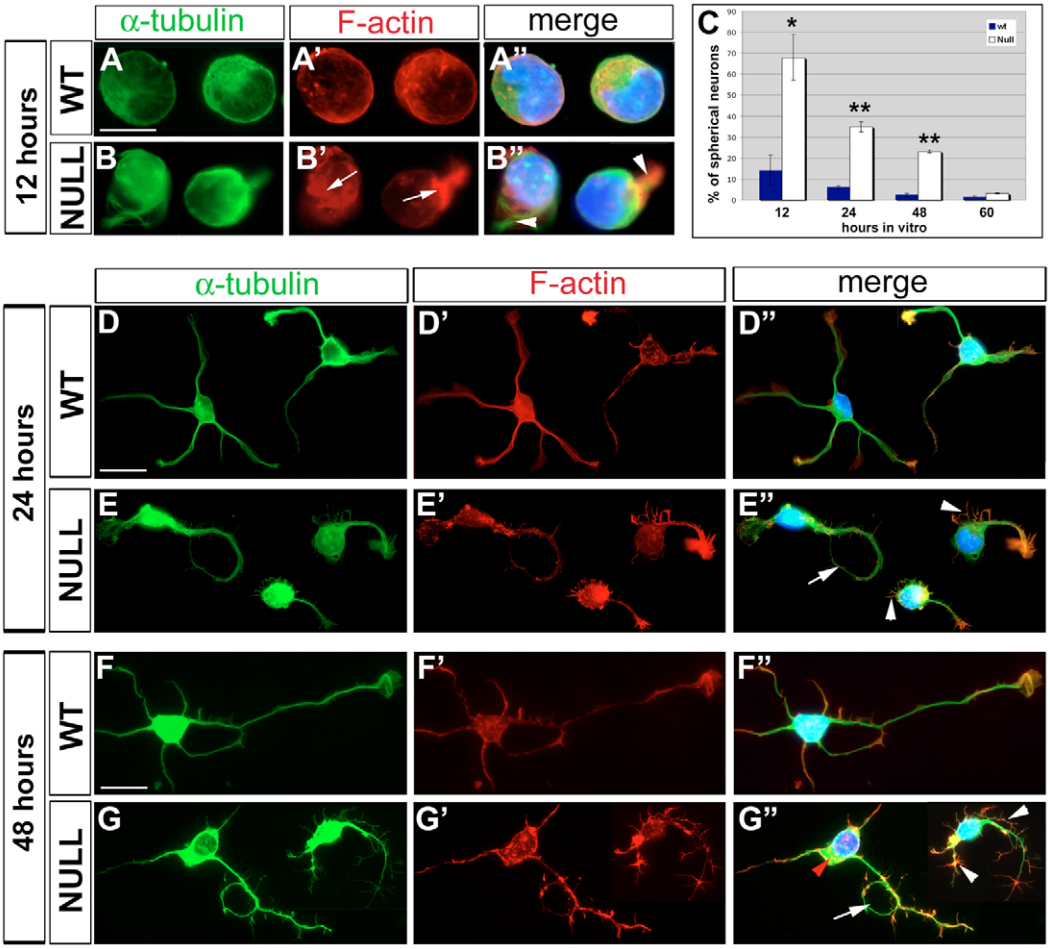

Fig. 6. Altered general morphology and morphometric parameters of *COUP-TFI*-deficient primary neurons. (A-G″) All the neurons were labelled with an antibody against tyrosinated α-tubulin (green) and rhodamine-phalloidin for actin (red). (A″-G″) Merged figures in which blue staining (DAPI) reveals the nucleus. (**A-B″**) After 12 hours of culture, *COUP-TFI*^{null} neurons show an abnormal distribution of actin filaments (arrows in B′) and no or very little protrusions (arrowheads in B″). (**C**) Graph showing the percentage of neurons that display a spherical phenotype at different hours after plating. (**D-E″**) After 24 hours in culture, *COUP-TFI*^{null} neurons have extended some neurites; however, they present a curled and abnormal growth pattern (arrow in E″). The arrowheads in E″ indicate the ectopic presence of protrusions. (**F-G″**) After 48 hours in culture most of the *COUP-TFI*^{null} neurons do have a more elongated axon; however, these neurons display numerous short filopodial extensions (arrowheads in G″), and axons tend to curl abnormally (arrow in G″). The red arrowhead indicates abnormal accumulation of tubulin- and actin-rich structures around the nucleus. Scale bars: 10 μm in A-B″; 20 μm in D-G″. NULL, *COUP-TFI*^{null} neurons; WT, wild-type neurons.

159.7±3.0 in null, P=0.05; MAP1B in axon, 130.7±5.0 in wild type versus 51.7±5.0 in null, P<0.001). Thus, in the absence of COUP-TFI, MAP1B levels are reduced in developing neurons.

Next, we performed immunofluorescence labelling of RND2 in wild-type and *COUP-TFI*^{null} pyramidal neurons to assess whether and how RND2 levels were upregulated in dissociated neurons. Localization of RND2 in hippocampal primary neurons has never been reported before. Staining of RND2 was mainly restricted to the cell body close to the pole where the axon elongates, as better seen in double immunofluorescence with TAU (Fig. 7D-D″). Surprisingly, RND2 was ectopically induced along the whole axon of *COUP-TFI*^{null} neurons (Fig. 7E-E″). Levels of RND2 upregulation were dependent on the degree of the morphological abnormalities present in COUP-TFI-deficient neurons (data not shown). Taken together, these data on dissociated neurons show that the abnormal levels of MAP1B and RND2 are mainly localized in growing axons in accordance with the abnormal axonal morphology described above.

DISCUSSION

An intrinsic in vivo role for COUP-TFI in differentiating the main forebrain commissural neurons

Our morphological analysis on *COUP-TFI* null brains shows various defects in the pathway of the major commissural projections. Callosal axons arrive at the midline but are unable to cross and swirl into longitudinal neuromas called Probst bundles, and aberrant fibres project abnormally along the AP axis. Similarly, hippocampal axons stop at the midline and project abnormally towards the AC. In addition, some AC fibres are misrouted towards the hippocampal commissure, although most fascicles do cross the midline. At first glance, these data could imply an intrinsic role for COUP-TFI in midline patterning or in regulating molecules required for midline crossing. At present we do not favour this hypothesis because COUP-TFI is expressed neither in the septum nor in the midline cells or glia, which have been shown to regulate the formation of midline commissures (Pires-Neto et al., 1998; Shu and Richards,

2001). Furthermore, expression levels of glial markers and guidance molecules, known to be involved in midline crossing (Shu et al., 2003; Zou et al., 2000), are not altered in *COUP-TFI* null embryos (data not shown). We therefore propose that the guidance pathfinding defects are intrinsic to the axons, which have severe axonal growth and formation defects, and might therefore be unable to project properly to their targets. Moreover, because of the expression of *COUP-TFI* in early born neurons in the presumptive cingulate cortex, we hypothesize that the defect might originate in pioneering axons that have been shown to guide later developing axons to their targets (Koester and O'Leary, 1994; Rash and Richards, 2001). This is the case for subplate cells, required for the formation of thalamocortical and corticofugal connections, which in the absence of *COUP-TFI* are abnormally differentiated (Zhou et al., 1999). Thus, abnormal neurite outgrowth and axonal morphology described in this study in primary dissociated neurons, might be reproduced in several populations of pioneer neurons, and could explain the broad axon guidance defects observed in *COUP-TFI* mutant mice.

In conclusion, it is plausible that COUP-TFI regulates the same group of molecules that are implicated in the development of all midline commissures (this study), and of corticothalamic and thalamocortical projections (unpublished observations) (Zhou et al., 1999). We propose that COUP-TFI acts intrinsically in regulating axonal outgrowth of several neuronal subpopulations rather than controlling other cell types required in guiding and positioning long-tract fibres in the forebrain.

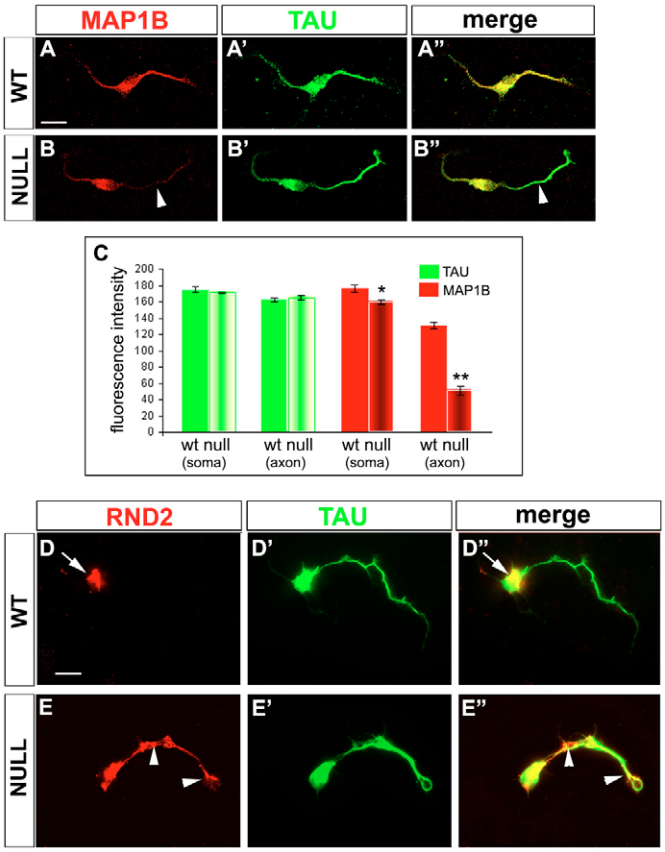

Fig. 7. Decreased MAP1B and increased RND2 levels in axons of COUP-TFI-deficient primary neurons. (**A-B″**) Confocal images of primary hippocampal neurons after 24 hours in culture labelled with antibodies recognizing MAP1B and TAU. MAP1B and TAU staining overlap in the cell body and neurites in wild-type neurons (A-A″). Axonal MAP1B levels are clearly reduced in *COUP-TFI*^{null} mutants, as shown by the arrowheads in B and in a merged image (B″), whereas TAU fluorescence levels do not change (B′). (**C**) Quantification of TAU and MAB1P fluorescence in the cell body and in the axon via relative intensity measurement (see text for more details). (**D-E″**) Immunofluorescence of RND2 and TAU in primary neurons after 48 hours in culture. RND2 is restricted to the cell body close to where the axon emerges in wild-type neurons, but is upregulated and ectopically distributed along the whole length of NULL neurons, as indicated by arrowheads (E-E″). Scale bars: 20 μm. NULL, *COUP-TFI*^{null} neurons; WT, wild-type neurons.

COUP-TFI regulates expression of microtubule- and actin-polymerizing factors implicated in neuron morphogenesis and axon outgrowth

This study shows for the first time that various molecules involved in the cytoskeleton machinery are affected in the absence of COUP-TFI. Two of these factors are microtubule-associated-molecules (MAPs) that contribute to the control of microtubule and actin stabilization and have important roles in neuronal development (reviewed by Dehmelt and Halpain, 2004). As shown by microarray analysis, real-time PCR and immunostaining, MAP1B transcript and protein levels are decreased in *COUP-TFI* mutant brains, whereas MAP2 shows a less dramatic downregulation. MAP1B is the first of the neuronal MAPs to be expressed during neuritogenesis, after which its expression is developmentally downregulated (Gonzalez-Billault et al., 2004). Cultured primary neurons from *MAP1B*-deficient mice show selective inhibition of axon formation that results in a delay in axon outgrowth (Gonzalez-Billault et al., 2001; Teng et al., 2001) and neurons tend to grow in a curled manner and exhibit growth-cone-turning abnormalities (Bouquet et al., 2004). Here, we show that *COUP-TFI*^{null} brains and primary hippocampal neurons have diminished MAP1B levels in growing axons and that primary neurons have delayed axon outgrowth and form loops and hairpin bends. Nevertheless, decreasing levels of MAP1B seem not to affect neuronal morphology, as shown in *MAP1B* heterozygous mutants, and homozygous *MAP1B* null mice have axon pathfinding defects that differ in some aspects to those observed in *COUP-TFI*^{null} mutants (Del Rio et al., 2004; Edelmann et al., 1996; Gonzalez-Billault et al., 2000; Meixner et al., 2000; Takei et al., 1997; Zhou et al., 1999) (A.M. and M.S., unpublished), suggesting that other molecules besides MAP1B might be affected in the phenotype observed in *COUP-TFI*^{null} mutants. In favour of this hypothesis are the findings that other genes implicated in axon formation have been found differentially expressed between wild-type and *COUP-TFI*^{null} brains. In particular, *Rnd2*, which belongs to the Rho-GTPase family and acts as a constitutively active GTP-bound protein, the activity of which is controlled at the transcriptional level (Foster et al., 1996; Nishi et al., 1999), is significantly upregulated in *COUP-TFI*^{null} brains and in mutant primary neurons, where expression becomes abnormally distributed along the axons. RND2 seems to be involved in the regulation of neuronal morphology through different effectors, such as neurite outgrowth inhibition with Pragmin and neurite branching with Rapostlin (Fujita et al., 2002; Tanaka et al., 2006). Rapostlin binds to the neural Wiskott-Aldrich syndrome protein (Kakimoto et al., 2004), which has been shown to stimulate actin polymerization and neuritogenesis, and the neural activity of which might be under the control of COUP-TFI (Le Page et al., 2004). Recently, it has been proposed that an in vivo function of RND2 is as a regulator of migration and morphological changes of cortical pyramidal neurons

(Nakamura et al., 2006). Interestingly, we show that the normal localization of RND2 in hippocampal pyramidal neurons is not uniform, but polarized in the cell body, suggesting an important role for RND2 in axonal morphogenesis. In the absence of COUP-TFI, RND2 levels increased massively and became distributed along the whole neuron, suggesting that COUP-TFI might be involved in restricting RND2 expression in the cell body. How this mechanism operates is still unknown, but will be of interest in future studies.

In summary, the abnormalities in the morphology of *COUP-TFI*^{null} hippocampal primary cells, together with the abnormal expression of proteins involved in the organization of the cytoskeleton, suggest a role for COUP-TFI in regulating genes involved in the cytoskeleton machinery. We hypothesize that the synergistic altered levels of MAP1B and RND2, in particular, and of MAP2 and CAP1 at a minor level, contribute to the phenotype observed in *COUP-TFI*^{null} neurons. Further experiments need to be performed in order to understand whether the COUP-TFI-mediated regulation of microtubule and actin cytoskeletal factors is direct or indirect.

We thank F. G. Rathjen for L1; A. Goffinet for Reelin; F. Propst for MAP1B; E. Soriano and J. Avila for SMI 31, MAP1B-125, GSK3, Ser-GSK3 and Tyr-GSK3; P. Lappalainen for CAP1 antibodies; P. Soriano for the DTA cassette; O. Marin for teaching us axonal tracing; D. Di Bernardo for helping in the microarray analysis; J. Avila and P. Salinas for suggestions in setting up the primary hippocampal culture; the TIGEM Transgenic and Knock-out Core facility; E. Giordano for animal husbandry; L. Richards for continuous suggestions; J. Avila, V. Castellani, P. Salinas and L. Puelles for comments on the manuscript; and the whole Studer laboratory for fruitful discussions. This work was supported by the Italian Telethon Foundation, by the Italian Ministry of Research (FIRB-MIUR-RBNE01WY7P; RBAU01RW82 and RBNE01BBYW) and by the European Community FP6 program under grant number LSHM-CT-2004-005139.

References

Baldi, P. and Long, A. D. (2001). A Bayesian framework for the analysis of microarray expression data: regularized *t*-test and statistical inferences of gene changes. *Bioinformatics* **17**, 509-519.
Banker, G. A. and Cowan, W. M. (1977). Rat hippocampal neurons in dispersed cell culture. *Brain Res.* **126**, 397-342.
Benjamini, Y. and Hochberg, Y. (1995). Controlling the false discovery rate: a practical and powerful approach to multiple testing. *J. R. Stat. Soc. B* **57**, 289-300.
Bertling, E., Hotulainen, P., Mattila, P. K., Matilainen, T., Salminen, M. and Lappalainen, P. (2004). Cyclase-associated protein 1 (CAP1) promotes cofilin-induced actin dynamics in mammalian nonmuscle cells. *Mol. Biol. Cell* **15**, 2324-2334.
Bouquet, C., Soares, S., von Boxberg, Y., Ravaille-Veron, M., Propst, F. and Nothias, F. (2004). Microtubule-associated protein 1B controls directionality of growth cone migration and axonal branching in regeneration of adult dorsal root ganglia neurons. *J. Neurosci.* **24**, 7204-7213.
Boyne, L. J., Martin, K., Hockfield, S. and Fischer, I. (1995). Expression and distribution of phosphorylated MAP1B in growing axons of cultured hippocampal neurons. *J. Neurosci. Res.* **40**, 439-450.
Bradke, F. and Dotti, C. G. (2000). Establishment of neuronal polarity: lessons from cultured hippocampal neurons. *Curr. Opin. Neurobiol.* **10**, 574-581.
Craig, A. M. and Banker, G. (1994). Neuronal polarity. *Annu. Rev. Neurosci.* **17**, 267-310.
Dehmelt, L. and Halpain, S. (2004). Actin and microtubules in neurite initiation: are MAPs the missing link? *J. Neurobiol.* **58**, 18-33.
Del Rio, J. A., Gonzalez-Billault, C., Urena, J. M., Jimenez, E. M., Barallobre, M. J., Pascual, M., Pujadas, L., Simo, S., La Torre, A., Wandosell, F. et al. (2004). MAP1B is required for Netrin 1 signaling in neuronal migration and axonal guidance. *Curr. Biol.* **14**, 840-850.
Dickson, B. J. (2002). Molecular mechanisms of axon guidance. *Science* **298**, 1959-1964.
Dotti, C. G., Sullivan, C. A. and Banker, G. A. (1988). The establishment of polarity by hippocampal neurons in culture. *J. Neurosci.* **8**, 1454-1468.
Edelmann, W., Zervas, M., Costello, P., Roback, L., Fischer, I., Hammarback, J. A., Cowan, N., Davies, P., Wainer, B. and Kucherlapati, R. (1996). Neuronal abnormalities in microtubule-associated protein 1B mutant mice. *Proc. Natl. Acad. Sci. USA* **93**, 1270-1275.
Fischer, I. and Romano-Clarke, G. (1990). Changes in microtubule-associated protein MAP1B phosphorylation during rat brain development. *J. Neurochem.* **55**, 328-333.
Foster, R., Hu, K. Q., Lu, Y., Nolan, K. M., Thissen, J. and Settleman, J. (1996). Identification of a novel human Rho protein with unusual properties: GTPase deficiency and in vivo farnesylation. *Mol. Cell. Biol.* **16**, 2689-2699.
Fujita, H., Katoh, H., Ishikawa, Y., Mori, K. and Negishi, M. (2002). Rapostlin is a novel effector of Rnd2 GTPase inducing neurite branching. *J. Biol. Chem.* **277**, 45428-45434.
Garel, S. and Rubenstein, J. L. (2004). Intermediate targets in formation of topographic projections: inputs from the thalamocortical system. *Trends Neurosci.* **27**, 533-539.
Gonzalez-Billault, C., Demandt, E., Wandosell, F., Torres, M., Bonaldo, P., Stoykova, A., Chowdhury, K., Gruss, P., Avila, J. and Sanchez, M. P. (2000). Perinatal lethality of microtubule-associated protein 1B-deficient mice expressing alternative isoforms of the protein at low levels. *Mol. Cell. Neurosci.* **16**, 408-421.
Gonzalez-Billault, C., Avila, J. and Caceres, A. (2001). Evidence for the role of MAP1B in axon formation. *Mol. Biol. Cell* **12**, 2087-2098.
Gonzalez-Billault, C., Engelke, M., Jimenez-Mateos, E. M., Wandosell, F., Caceres, A. and Avila, J. (2002). Participation of structural microtubule-associated proteins (MAPs) in the development of neuronal polarity. *J. Neurosci. Res.* **67**, 713-719.
Gonzalez-Billault, C., Jimenez-Mateos, E. M., Caceres, A., Diaz-Nido, J., Wandosell, F. and Avila, J. (2004). Microtubule-associated protein 1B function during normal development, regeneration, and pathological conditions in the nervous system. *J. Neurobiol.* **58**, 48-59.
Goold, R. G. and Gordon-Weeks, P. R. (2001). Microtubule-associated protein 1B phosphorylation by glycogen synthase kinase 3beta is induced during PC12 cell differentiation. *J. Cell Sci.* **114**, 4273-4284.
Goold, R. G. and Gordon-Weeks, P. R. (2005). The MAP kinase pathway is upstream of the activation of GSK3beta that enables it to phosphorylate MAP1B and contributes to the stimulation of axon growth. *Mol. Cell Neurosci.* **28**, 524-534.
Johnstone, M., Goold, R. G., Bei, D., Fischer, I. and Gordon-Weeks, P. R. (1997). Localisation of microtubule-associated protein 1B phosphorylation sites recognised by monoclonal antibody SMI-31. *J. Neurochem.* **69**, 1417-1424.
Jouandet, M. L. and Hartenstein, V. (1983). Basal telencephalic origins of the anterior commissure of the rat. *Exp. Brain Res.* **50**, 183-192.
Kakimoto, T., Katoh, H. and Negishi, M. (2004). Identification of splicing variants of Rapostlin, a novel RND2 effector that interacts with neural Wiskott-Aldrich syndrome protein and induces neurite branching. *J. Biol. Chem.* **279**, 14104-14110.
Kalcheva, N., Albala, J., O'Guin, K., Rubino, H., Garner, C. and Shafit-Zagardo, B. (1995). Genomic structure of human microtubule-associated protein 2 (MAP-2) and characterization of additional MAP-2 isoforms. *Proc. Natl. Acad. Sci. USA* **92**, 10894-10898.
Koester, S. E. and O'Leary, D. D. (1994). Axons of early generated neurons in cingulate cortex pioneer the corpus callosum. *J. Neurosci.* **14**, 6608-6620.
Kutschera, W., Zauner, W., Wiche, G. and Propst, F. (1998). The mouse and rat MAP1B genes: genomic organization and alternative transcription. *Genomics* **49**, 430-436.
Le Page, Y., Demay, F. and Salbert, G. (2004). A neural-specific splicing event generates an active form of the Wiskott-Aldrich syndrome protein. *EMBO Rep.* **5**, 895-900.
Liu, Q., Dwyer, N. D. and O'Leary, D. D. (2000). Differential expression of COUP-TFI, CHL1, and two novel genes in developing neocortex identified by differential display PCR. *J. Neurosci.* **20**, 7682-7690.
Livak, K. J. and Schmittgen, T. D. (2001). Analysis of relative gene expression data using real-time quantitative PCR and the 2(–Delta Delta C(T)) Method. *Methods* **25**, 402-408.
Lopez-Bendito, G. and Molnar, Z. (2003). Thalamocortical development: how are we going to get there? *Nat. Rev. Neurosci* **4**, 276-289.
Medina, L., Legaz, I., Gonzalez, G., De Castro, F., Rubenstein, J. L. and Puelles, L. (2004). Expression of Dbx1, Neurogenin 2, Semaphorin 5A, Cadherin 8, and Emx1 distinguish ventral and lateral pallial histogenetic divisions in the developing mouse claustroamygdaloid complex. *J. Comp. Neurol.* **474**, 504-523.
Meixner, A., Haverkamp, S., Wassle, H., Fuhrer, S., Thalhammer, J., Kropf, N., Bittner, R. E., Lassmann, H., Wiche, G. and Propst, F. (2000). MAP1B is required for axon guidance and is involved in the development of the central and peripheral nervous system. *J. Cell Biol.* **151**, 1169-1178.
Nakamura, K., Yamashita, Y., Tamamaki, N., Katoh, H., Kaneko, T. and Negishi, M. (2006). In vivo function of Rnd2 in the development of neocortical pyramidal neurons. *Neurosci. Res.* **54**, 149-153.
Nishi, M., Takeshima, H., Houtani, T., Nakagawara, K., Noda, T. and Sugimoto, T. (1999). RhoN, a novel small GTP-binding protein expressed predominantly in neurons and hepatic stellate cells. *Brain Res. Mol. Brain Res.* **67**, 74-81.
Park, J. I., Tsai, S. Y. and Tsai, M. J. (2003). Molecular mechanism of chicken ovalbumin upstream promoter-transcription factor (COUP-TF) actions. *Keio J. Med.* **52**, 174-181.

Pires-Neto, M. A., Braga-De-Souza, S. and Lent, R. (1998). Molecular tunnels and boundaries for growing axons in the anterior commissure of hamster embryos. *J. Comp. Neurol.* **399**, 176-188.
Qiu, Y., Pereira, F. A., DeMayo, F. J., Lydon, J. P., Tsai, S. Y. and Tsai, M. J. (1997). Null mutation of mCOUP-TFI results in defects in morphogenesis of the glossopharyngeal ganglion, axonal projection, and arborization. *Genes Dev.* **11**, 1925-1937.
Rash, B. G. and Richards, L. J. (2001). A role for cingulate pioneering axons in the development of the corpus callosum. *J. Comp. Neurol.* **434**, 147-157.
Shu, T. and Richards, L. J. (2001). Cortical axon guidance by the glial wedge during the development of the corpus callosum. *J. Neurosci.* **21**, 2749-2758.
Shu, T., Sundaresan, V., McCarthy, M. M. and Richards, L. J. (2003). Slit2 guides both precrossing and postcrossing callosal axons at the midline in vivo. *J. Neurosci.* **23**, 8176-8184.
Takei, Y., Kondo, S., Harada, A., Inomata, S., Noda, T. and Hirokawa, N. (1997). Delayed development of nervous system in mice homozygous for disrupted microtubule-associated protein 1B (MAP1B) gene. *J. Cell Biol.* **137**, 1615-1626.
Tanaka, H., Katoh, H. and Negishi, M. (2006). Pragmin, a novel effector of Rnd2 GTPase, stimulates RhoA activity. *J. Biol. Chem.* **281**, 10355-10364.
Teng, J., Takei, Y., Harada, A., Nakata, T., Chen, J. and Hirokawa, N. (2001). Synergistic effects of MAP2 and MAP1B knockout in neuronal migration, dendritic outgrowth, and microtubule organization. *J. Cell Biol.* **155**, 65-76.
Tripodi, M., Filosa, A., Armentano, M. and Studer, M. (2004). The COUP-TF nuclear receptors regulate cell migration in the mammalian basal forebrain. *Development* **131**, 6119-6129.
Ulloa, L., Diaz-Nido, J. and Avila, J. (1993). Depletion of casein kinase II by antisense oligonucleotide prevents neuritogenesis in neuroblastoma cells. *EMBO J.* **12**, 1633-1640.
Zhou, C., Qiu, Y., Pereira, F. A., Crair, M. C., Tsai, S. Y. and Tsai, M. J. (1999). The nuclear orphan receptor COUP-TFI is required for differentiation of subplate neurons and guidance of thalamocortical axons. *Neuron* **24**, 847-859.
Zhou, C., Tsai, S. Y. and Tsai, M. J. (2001). COUP-TFI: an intrinsic factor for early regionalization of the neocortex. *Genes Dev.* **15**, 2054-2059.
Zou, Y., Stoeckli, E., Chen, H. and Tessier-Lavigne, M. (2000). Squeezing axons out of the gray matter: a role for slit and semaphorin proteins from midline and ventral spinal cord. *Cell* **102**, 363-375.